Received: 5 June 2023 | Revised: 7 December 2023 | Accepted: 10 December 2023

DOI: 10.1111/all.15998

Allergy EUROPEAN JOURNAL OF ALLERGY AND CLINICAL IMMUNOLOGY EAACI WILEY

ORIGINAL ARTICLE

Propionate alleviates itch in murine models of atopic dermatitis by modulating sensory TRP channels of dorsal root ganglion

Yao Xu[1] | Zhuoqiong Qiu[1] | Chaoying Gu[1] | Su Yu[1] | Shangshang Wang[1] | Changlin Li[2] | Xu Yao[3] | Wei Li[1]

[1]Department of Dermatology, Huashan Hospital, Fudan University, Shanghai Institute of Dermatology, Shanghai, China

[2]Guangdong Institute of Intelligence Science and Technology, Zhuhai, China

[3]Department of Allergy and Rheumatology, Jiangsu Key Laboratory of Molecular Biology for Skin Diseases and STIs, Hospital for skin diseases, Institute of Dermatology, Chinese Academy of Medical Sciences and Peking Union Medical College, Nanjing, China

Correspondence
Wei Li, Department of Dermatology, Huashan Hospital, Fudan University, 12 Wulumuqi Middle Road, Shanghai 200040, China.
Email: liweiderma@fudan.edu.cn

Xu Yao, Department of Allergy and Rheumatology, Institute of Dermatology, Chinese Academy of Medical Sciences and Peking Union Medical College, 12 Jiangwangmiao Street, Nanjing 210042, China.
Email: dryao_xu@126.com

Funding information
Nanjing Incubation Program for National Clinical Research Centre; Key Project of the Innovation Program of Shanghai Municipal Education Commission, Grant/Award Number: 2021-01-07-00-07-E00078; Shanghai Municipal Commission of Health and Family Planning; Key Project of Social Development in Jiangsu Province; Milstein Medical Asian American Partnership Foundation; Shanghai Municipal Key Clinical Specialty, Grant/Award Number: shslczdzk01002; National Natural Science Foundation of China, Grant/Award Number: 82073446, 81972939, 82273531, 82003349, 82003357 and 82330098

Abstract

Background: Itch is the most common symptom of atopic dermatitis (AD) and significantly decreases the quality of life. Skin microbiome is involved in AD pathogenesis, whereas its role in the regulation of itch remains elusive. In this study, we aimed to investigate the effects of skin microbial metabolite propionate on acute and chronic pruritus and to explore the mechanism.

Methods: Using various mouse models of itch, the roles of propionate were explored by behavioral tests and histopathology/immunofluorescent analysis. Primary-cultured dorsal root ganglion neurons and HEK293 cells expressing recombinant human TRP channels were utilized for in vitro calcium imaging/in vivo miniature two-photon imaging in combination with electrophysiology and molecular docking approaches for investigation of the mechanism.

Results: Propionate significantly alleviated itch and alloknesis in various mouse models of pruritus and AD and decreased the density of intraepidermal nerve fibers. Propionate reduced the responsiveness of dorsal root ganglion neurons to pruritogens in vitro, attenuated the hyper-excitability in sensory neurons in MC903-induced AD model, and inhibited capsaicin-evoked hTRPV1 currents ($IC_{50} = 20.08 \pm 1.11\,\mu M$) via interacting with the vanilloid binding site. Propionate also decreased the secretion of calcitonin gene-related peptide by nerves in MC903-induced AD mouse model, which further attenuated itch and skin inflammation.

Conclusion: Our study revealed a protective effect of propionate against persistent itch through direct modulation of sensory TRP channels and neuropeptide production in neurons. Regulation of itch via the skin microbiome might be a novel strategy for the treatment of AD.

Abbreviations: AD, atopic dermatitis; AITC, allyl-isothiocyanate; CGRP, calcitonin gene-related peptide; CQ, chloroquine; DRG, dorsal root ganglion; GPR41, G protein-coupled receptors 41; HDAC, histone deacetylase; IL-4, interleukin 4; MC903, calcipotriol; SCFA, short-chain fatty acids; Th2, T helper 2 cell; Treg, regulatory T cells; TSLP, thymic stromal lymphopoietin; TRPA1, transient receptor potential ankyrin 1; TRPM8, transient receptor potential melastatin 8; TRPV1, transient receptor potential vanilloid 1; 5-HT, 5-hydroxytryptamine.

KEYWORDS
atopic dermatitis, calcitonin gene-related peptide, dorsal root ganglion, itch, propionate, skin microbiome metabolite, TRP channels

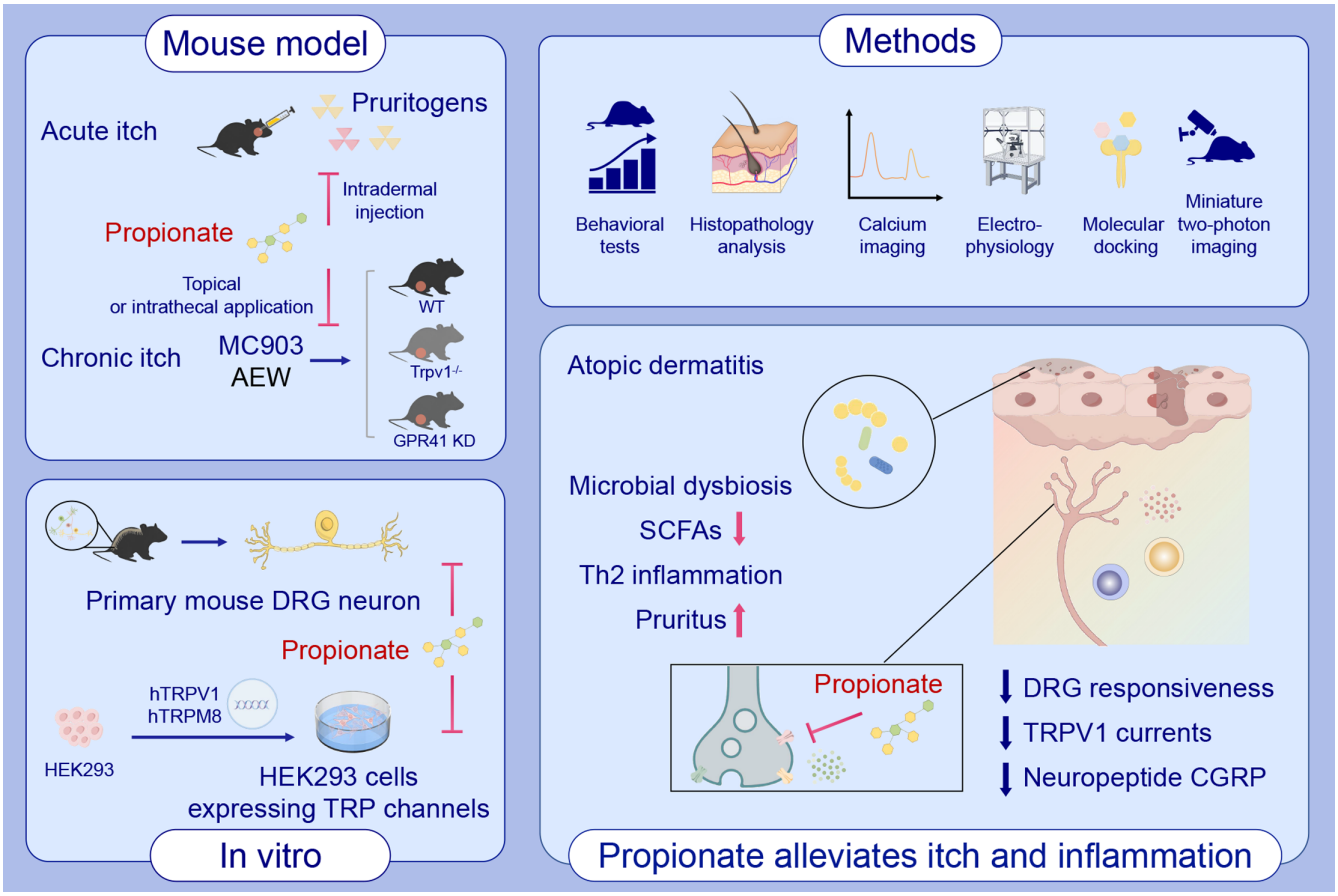

GRAPHICAL ABSTRACT

Skin microbial metabolite propionate alleviates itch and skin inflammation. Propionate reduces the responsiveness of DRG neurons to pruritogens, directly modulates sensory TRP channels, and inhibits the secretion of neuropeptide CGRP. Regulation of itch via the skin microbiome might be a novel strategy for the treatment of AD. Abbreviations: AD, atopic dermatitis; AEW, acetone-ether-water; CGRP, calcitonin gene-related peptide; DRG, dorsal root ganglion; GPR41, G protein-coupled receptor 41; HEK293, human embryonic kidney cell line; KD, knockdown; MC903, calcipotriol; SCFAs, short chain fatty acids; Th2, T helper 2 cell; TRPV1, transient receptor potential vanilloid 1; WT, wild type.

1 | INTRODUCTION

Atopic dermatitis (AD) is a chronic, recurrent, inflammatory skin disease, with itch as the most predominant symptom that significantly decreases the quality of life.[1,2] Type 2 inflammation, epidermal barrier dysfunction, and skin microbial dysbiosis play important roles in the pathogenesis of AD and are differentially involved in elicitation of itch.[3,4] Skin lesion of AD is hyperinnervated by primary somatosensory afferent neurons, mainly myelinated A-fibers and unmyelinated C-fibers, originating from the dorsal root ganglion (DRG) or the trigeminal ganglia (TG).[5] The nerve terminals penetrating into the epidermis may interact with a diverse array of pruritogens released by keratinocytes, immune cells, and the skin microbiota.[6] Many type 2 cytokines, such as interleukin (IL)-4, IL-13, IL-31, IL-33, and thymic Stromal Lymphopoietin (TSLP), can induce itch by binding to their irrespective receptors expressing on sensory nerves[7] and may enhance the sensitiveness to other pruritogens.[8] These cytokines are also responsible for the elongation and sprouting of nerve fibers, which are associated with persistent itch.[9,10] However, the regulation on itch in AD is far less recognized and awaits extensive exploration.

Skin microbiome participates in the pathogenesis of AD in various aspects.[11–13] The features of skin microbial dysbiosis in AD include increased abundance of *Staphylococcus aureus* (*S. aureus*) and decreased abundance of commensal bacteria such as *Cutibacterium acnes* (the former *Propionibacterium acnes*).[14,15] Studies have reported that *S. aureus* not only promotes skin inflammation and impairs epidermal barrier function, but also induces itch. Proteases secreted by *S. aureus* bind to the protease-activated receptors (PAR-2 and PAR-4) on nerves and elicit itch[16]; mas-related G protein coupled receptors X2 (MRGPRX2) expressing in peripheral sensory neurons and mast

cells can be activated by microbial pathogen-induced production of anti-microbial peptides (AMPs) to promote the release of IL-31.[17] On the other hand, skin commensals exert protective effects in AD by killing of *S. aureus*, inhibition of skin inflammation, or promotion of barrier recovery.[12,13,18] Nevertheless, the regulatory effect of skin commensal on itch remains elusive. We recently reported that the production of sebum was decreased in AD patients, and the level of propionate, a microbial metabolite of sebum, was also significantly decreased on the skin surface, which participated in the regulation of skin inflammation by inhibiting the production of IL-33 in keratinocytes.[19] Short-chain fatty acids (SCFAs) have been reported involving in the gut-brain axis through complex neuro-immune communications,[20] by activating free fatty acid receptors (FFARs) or inhibiting histone deacetylases (HDACs).[21] Moreover, SCFAs can regulate secretions of neurotransmitters and directly activate vagal afferents, thereby affecting food-intake, learning, memory, and emotion.[22] However, whether SCFAs play a role in modulation of itch is not clear.

The transient receptor potential (TRP) family are frequently considered as key common downstream channel of both histaminergic and non-histaminergic itch.[5] Transduction of electrical impulse requires the open TRP channels on nociceptors, which is subsequently relayed to brain and processed as itch sensation and elicit scratching behavior.[23] Multiple pieces of evidence have demonstrated that TRPV1 and TRPA1 contribute to the transduction of inflammation-induced noxious stimuli in sensory neurons. TRPV1 channel agonists (capsaicin, RTX), have been utilized to desensitize sensory neurons and reduce neurogenic inflammation for treatment of pain or itch in the context of multiple skin diseases. The neuro-immune crosstalk is bidirectional, and sensory afferents not only transmit conscious perception, but also regulate immune responses in an efferent manner via neuropeptides.[24] Among them, calcitonin gene-related peptide (CGRP) has drawn extensive attention, which profoundly augments type 2 immune responses,[25,26] and CGRP-positive nerve fibers are increased in the skin lesions of AD patients.[27] Thus, modulation of CGRP production by nerves would be beneficial for the regulation of the skin inflammation in AD.

In the current study, we utilized multifaceted approaches and demonstrated an antipruritic effect of propionate in multiple mouse models of itch. Calcium imaging and electrophysiological recordings were performed on DRGs and HEK293 cells expressing specific ion channels, and propionate was defined as a modulator of sensory TRPs. Our data revealed that propionate protected against persistent itch and skin inflammation through dampening neuronal excitability as well as inhibiting the release of neuropeptide CGRP, providing basis for novel therapeutic strategies for itch.

2 | RESULTS

2.1 | Propionate alleviates acute and chronic itch

We first assessed the effects of propionate on acute itch. The cheek assay was applied to distinguish itch from pain behaviors, in which 8-week-old mice were intradermally injected with pruritogens in the cheek, and hind paw scratching bouts of the injection site were video-recorded and calculated. The results showed that histamine (100 μg), chloroquine (50 μg), compound 48/80 (20 μg), and 5-HT (2 μg) successfully elicited acute itch-like behavior in the mice (Figure 1A–D). Intradermal pre-injection of 4 mM propionate 30 min ahead of time markedly reduced the numbers of scratching induced by histamine ($p = .0014$), chloroquine ($p = .035$), and compound 48/80 ($p = .0006$), but not 5-HT ($p = .84$), compared with vehicle control (Figure 1A–D).

For evaluation of the role of propionate in chronic itch, the MC903-induced mouse model of AD was produced (Figure 1E).[8] MC903 was applied on the ears of mice for 9 consecutive days, and an increasing amount of scratching bouts was observed, which was attenuated by topical application with 4 mM propionate (Figure 1F). The severity of skin lesions was also remarkably reduced in the MC903 mice treated with propionate compared to that treated with vehicle control in a dose-dependent manner, as shown by decreased erythema, edema, dryness, and ear epidermal thickness in the MC903 plus propionate group ($p < .0001$, Figure 1G,H; $p = .0005$, Figure 1I,J; Figure S1). Moreover, immunofluorescence showed that the increase in intraepidermal nerve fiber density (IENFD) in the MC903-treated mice was attenuated upon propionate treatment ($p = .0074$, Figure 1K,L). These data suggested that propionate inhibited both acute and inflammatory chronic itch.

2.2 | Propionate alleviates non-inflammatory chronic itch and alloknesis

To discriminate the effects of propionate on itch from inflammation, we assessed the effects of propionate in a xerosis model that was produced by application with a mixture of acetone, ether, and water (AEW)[28] on the mouse dorsal skin (Figure 2A). At each time point, the robust spontaneous scratches in the AEW model were significantly attenuated upon topical propionate treatment (Figure 2B). Similarly, propionate application also improved the overall conditions and pathological injury of the AEW model, as shown by the decreased dermatitis score and epidermal thickness (Figure 2C–F). Moreover, the density of epidermis nerve fiber in the AEW mice was increased compared with that in controls ($p = .0010$). Propionate treatment moderately decreased intraepidermal nerve fiber density, but without statistical significance (Veh vs. Pro, $p = .065$, Figure 2G,H).

Intrathecal delivery of propionate was then performed to exclude the possibility that SCFAs may act through skin resident cells, such as keratinocytes and immune cells (Figure 2I).[20] Notably, the chronic itch induced by MC903 or AEW and alloknesis evoked by light touch around the lesions were all alleviated by daily intrathecal injection with 1 mM propionate (Figure 2J,K). Besides, the expressions of Th2 cytokines and regulatory cytokines were also reduced in the skin of MC903 mice treated with propionate, except TSLP (Figure S2A). In AEW mice, only the levels of IL-31, IL-33, and TSLP were increased in skin lesions, which were decreased after propionate treatment (Figure S2B). No spontaneous pruritus or hypersensitivity in mice

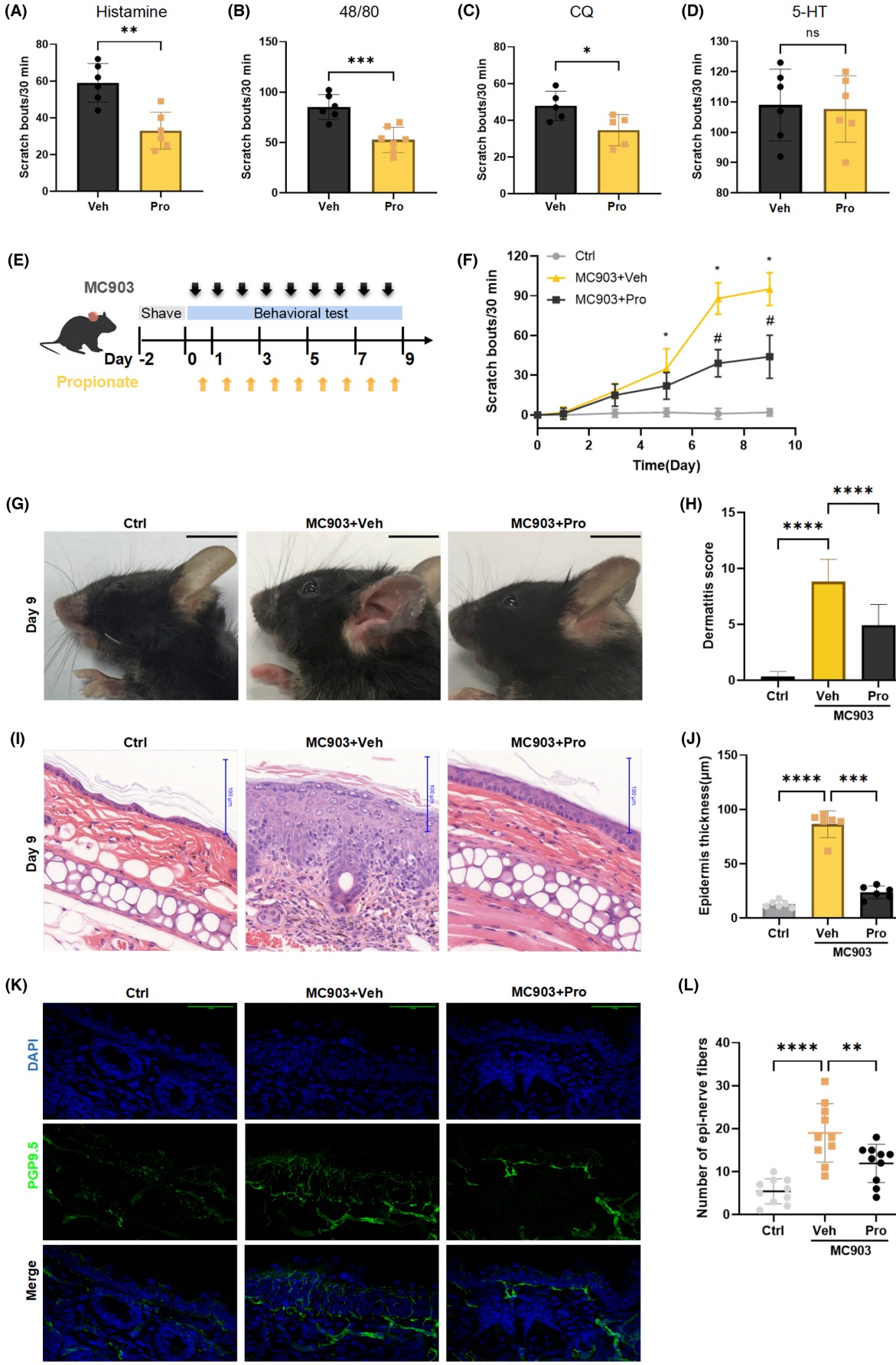

FIGURE 1 Propionate inhibits acute and chronic itch. (A–D) Cheek-directed scratching bouts induced by intradermal injection of histamine, 48/80, chloroquine, or 5-HT in mice treated with propionate or vehicle control ($n = 5–6$ mice). (E) Experimental schema of daily topical applications with MC903, propionate, or vehicle. (F) Time courses of the numbers of spontaneous scratching bouts among different groups. (G, H) Gross appearance of skin lesion. Representative images of skin lesions are shown in (G) (Scale bar = 1 cm), and statistical result for dermatitis scores of each group is shown in (H). (I, J) Histopathology of skin tissues. Results of H&E staining are shown in (I) (Scale bar = 100 μm), and statistical result for epidermis thickness of each group is shown in (J). (K, L) Immunofluorescence of nerve fibers. Representative immunofluorescent images of cutaneous peripheral nerve fibers stained with PGP9.5 (green) and DAPI (blue) are shown in (K) (Scale bar = 50 μm). Statistical result for the calculation of intradermal PGP9.5-positive nerves of each group is shown in (L). Data are represented as mean ± SEM, $n = 6$ mice/group, two-tailed unpaired Student's *t*-test was applied (A–D), two-way ANOVA followed by Tukey honest significant difference post hoc test (F), one-way ANOVA followed by Fisher's least significant difference post hoc correction for multiple comparisons (H, J, L), ns, no significance, $^{*}p < .05$, $^{**}p < .01$, $^{***}p < .001$ and $^{****}p < .0001$. Ctrl, control; Pro, propionate; Veh, vehicle control.

treated with propionate only was noticed, and no motor impairment was detected as assessed by rotarod tests (Figure S3A). As certain noxious stimulus may cause a transient relief on itch, we performed Von Frey and Hargreaves trails to evaluate whether propionate was involved in nociception. The result showed that there was no significant difference in paw withdrawal threshold or latency to mechanical/heat stimulus between the mice receiving intrathecal injection of 1 mM propionate and vehicle. No pain-like behaviors, such as licking or flicking, were observed after paw injection of 4 mM propionate within the first 5 min (Figure S3B,C). Thus, the antipruritic effect of propionate might result from the direct regulation by propionate on sensory neurons, which affected neither mechanical nor thermal pain sensitivity at the given dosage.

2.3 | Propionate directly regulates activation of DRG neuron

Next, we tested the direct effect of propionate on DRG by assessing the responsiveness of in vitro cultured DRG via calcium imaging. When exposed to successive pruritogens, approximately 11.2%, 8.34%, 28.11%, and 41.78% of total KCL-responsive DRG neurons (confirming viability) responded to histamine, menthol, AITC, and capsaicin, respectively (Figure 3A,B), which were comparable to previous findings.[29] While mostly, propionate did not activate DRG neurons directly. Application of 1 mM propionate alone only led to calcium influx in around 1.58% of DRG neurons (Figure 3B, Figure S4A,B).

Then we investigated whether propionate could alter the responsiveness of DRG neurons to other pruritogens. When exposed to multiple challenges after incubated with 100 μM propionate, the frequency and peak amplitude of sensory neurons responding to type 2 cytokine IL-4 ($p = .031$) and capsaicin ($p < .0001$) were significantly decreased compared to medium (Figure 3C,D,H, Figure S4C–F). Conversely, we observed a somewhat increased calcium peak, but not increase in the percentage of DRG neurons, triggered by menthol after treatment with propionate ($p = .95$, Figure 3E,H,I). As for acute pruritogens, two consecutive exposures to histamine or chloroquine evoked consistent calcium influx; however, when pre-applied with propionate, the second peak was markedly lower than the first one (Figure 3F,G,H,I). Whereas the calcium response to AITC stimulation was almost unaffected after propionate application ($p = .20$, Figure 3H,I). In addition, the transcriptional expressions of TRPV1, TRPA1, TRPM8, and Mrgprd were up-regulated in the DRG neurons from spinal segments corresponding to the skin lesions in MC903 mice, but there were no differences between the groups treated with propionate and vehicle (Figure 3J). These results illustrated that propionate did not influence the expression of ion channels at transcript level but exerted its effects on the functional states of DRG. Collectively, our data indicated that propionate played a functional modulatory role in DRG neurons, which might be through sensory TRP channels.

2.4 | Propionate attenuates MC903-induced hyper-excitability in sensory neurons

Based on the inhibitory effects of propionate on calcium responses of DRG, we hypothesized that the excitability of DRG neurons might also be affected by propionate. To test this possibility, current clamp recording was performed on small diameter DRG neurons that mainly correspond to nociceptors.[8] The result showed that when injected with the same amplitude of step current, DRG neurons from the MC903 mice treated with vehicle fired much more action potentials compared with those from control mice, as shown in the representative traces (Figure 4A,B). Importantly, the frequency of firing in response to 1 s, 0–250 pA depolarizing current was potently reduced in DRGs from the MC903 mice intrathecally injected with 1 mM propionate. Furthermore, we found that the current threshold required for eliciting the first action potential was clearly decreased, as suggested by the hyper-excitability of sensory neurons in the MC903 mice treated with vehicle ($p = .008$), while propionate restored the rheobase as expected ($p = .0031$, Figure 4C). Besides, no significant difference was detected in resting membrane potential ($p = .37$, Figure 4D) and peak amplitude ($p = .34$, Figure 4E).

Next, we explored the dorsal horn neural activity using in vivo calcium imaging. Since subtle responses of sensory neurons might be obscured by anesthesia, miniature two-photon microscope was adopted to track neuronal activity under freely behaving conditions and monitor large-scale calcium transients in real-time. After

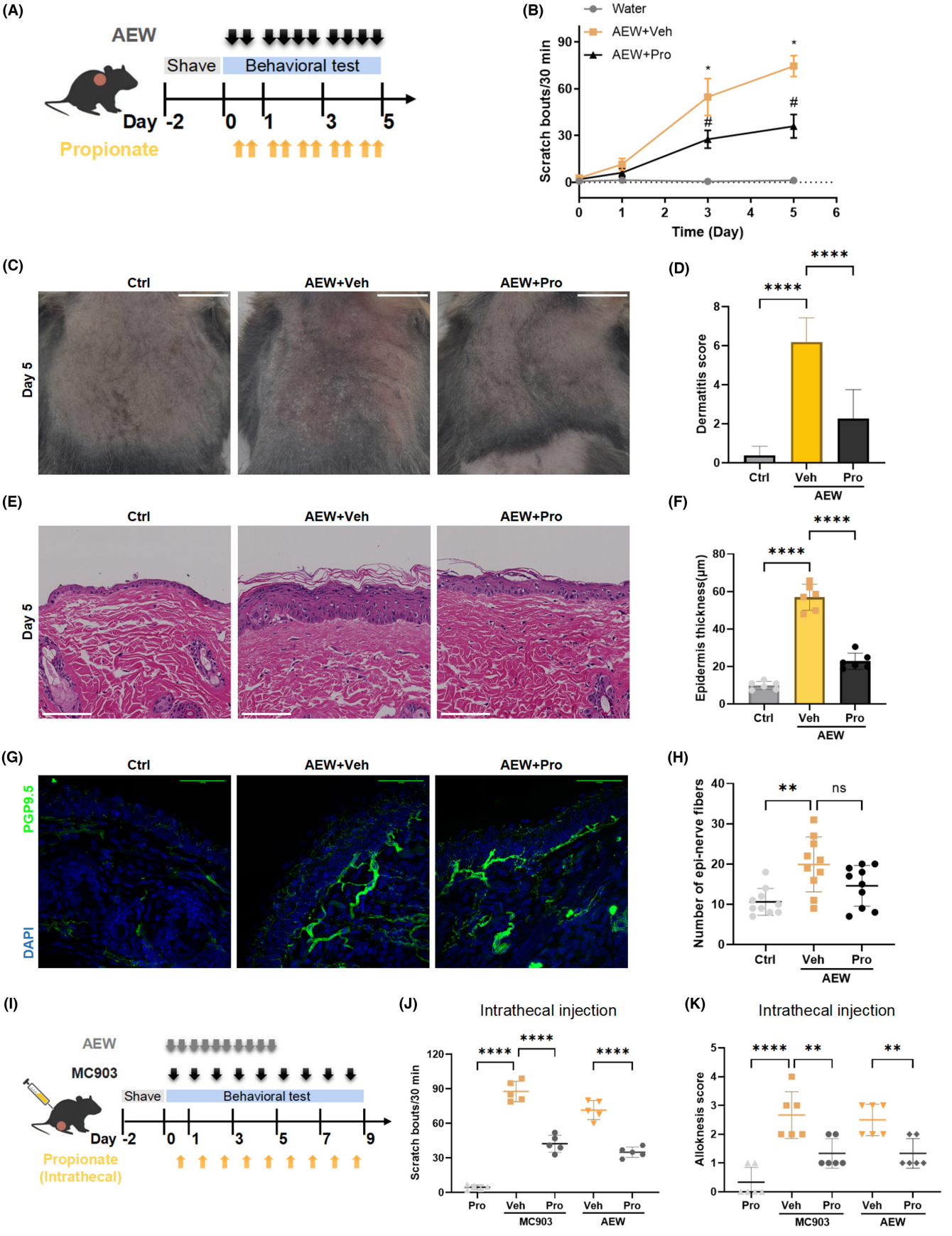

FIGURE 2 Propionate alleviates AEW-induced itch and alloknesis in mice. (A) Experimental schema of daily topical applications with AEW, propionate, or vehicle. (B) Time courses of the numbers of spontaneous scratching bouts among different groups. (C, D) Gross appearance of skin lesion. Representative images of skin lesions are shown in (C) (Scale bar = 1 cm), and statistical result for dermatitis scores of each group is shown in (D). (E, F) Histopathology of skin tissues. Results of H&E staining are shown in (E) (Scale bar = 100 μm), and statistical result for epidermis thickness of each group is shown in (F). (G, H) Immunofluorescence of nerve fibers. Representative immunofluorescent images of cutaneous peripheral nerve fibers stained with PGP9.5 (green) and DAPI (blue) are shown in (G) (Scale bar = 50 μm). Statistical result for calculation of intradermal PGP9.5-positive nerves of each group is shown in (H). (I) Experimental schema of daily intrathecal injection with propionate (1 nM) or vehicle in AEW or MC903 mice. (J) Numbers of spontaneous scratching bouts among different groups. (K) Alloknesis scores in mice with intrathecal injection of propionate or vehicle control. Data are represented as mean ± SEM, $n = 6$ mice/group, two-way ANOVA followed by Tukey honest significant difference post hoc test (B), one-way ANOVA followed by Fisher's least significant difference post hoc correction for multiple comparisons (D, F, H, J, K), ns = no significance, $^{*}p < .05$, $^{**}p < .01$ and $^{****}p < .0001$. AEW, acetone-ether-water; Ctrl, control; Pro, propionate; Veh, vehicle control. See also Figures S2 and S3.

inducing the expression of GCaMP6s via adeno-associated viruses (AAV) injection, MC903 was applied to the hindlimb skin within the innervation region of spinal dorsal horn (See Videos S1 and S2). Corresponding to the reduced itch behaviors, we observed that the frequency and intensity of calcium transients of labeled neurons were significantly lower in propionate-treated MC903 mice, compared with vehicle controls (Figure 4F). Then we used tape response assay to characterize the hyperreaction to innocuous stimuli in AD.[30] When an adhesive tape was attached to the skin lesions, the MC903 mice from vehicle group showed obviously more attempts to remove the tape as well as increased spontaneous calcium firing, which were strongly suppressed by propionate application (Figure 4G).

It has been reported that SCFAs activate vagal afferents through G protein-coupled receptors FFAR3 (GPR41).[22] In order to determine the involvement of this receptor in propionate-mediated pruritus inhibition, we forced GPR41-knockdown in DRG via intrathecal delivery of AAV2/9 carrying GPR41-shRNA or GPR41-sc (Figure S5A). The result showed that the protective role of propionate in itch elicitation and skin inflammation induction was not abolished by GPR41-silencing in either MC903 or AEW model (Figure S5B,C). We also found that the expression levels of GPR41 mRNA transcripts in skin and DRG were extremely low, or even undetectable as quantified by qPCR (Figure S5D), which was consistent with a recent study exploring the GPR41 expressions in mice.[31] There was no difference in the reduction of the calcium influx frequency and peak amplitude induced by propionate in capsaicin-responsive neurons among GPR41 knockdown groups (Figure S5E–G). Therefore, we speculated that the antipruritic effects of propionate might be independent of GPR41.

2.5 | Propionate reversibly modulates hTRPV1 and hTRPM8 channel activity

Since propionate was closely linked to sensory TRP channels TRPV1 and TRPM8, we then evaluated the effects of propionate on HEK 293 cells expressing recombinant hTRPV1 and hTRPM8. As expected, 50 μM propionate directly evoked intracellular Ca^{2+} responses in hTRPM8-transfected cells (Figure 5A,B). Subsequent stimulation with 100 μM menthol caused an even stronger calcium influx, while no responses were observed when application of 50 μM propionate was repeated within the following 10 min; however, repetitive stimulation with menthol still induced similar responses as before, indicating the recovery of channel activity (Figure 5A,B). These results implicated that propionate-responsive neurons overlapped with menthol-responsive neurons to a great extent and propionate might be a partial agonist of TRPM8.

Similar to what we have learned from DRG neurons, 30 s pretreatment of propionate resulted in obvious hTRPV1 desensitization responding to capsaicin, the second peak was markedly lower than the first one (Figure 5C). While after sufficient washout, subsequent capsaicin administration could elicit a moderate calcium peak again in the absence of propionate (Figure 5C). Notably, the interspersed washing period in our paradigm was enough for the recovery of TRPV1 channel, as evidenced by the similar amplitude of calcium peak primed by the second capsaicin stimulation (Figure 5D). Interestingly, continuous incubation with 500 μM propionate followed by subsequent repeated administrations of 300 nM capsaicin no longer induced any calcium responses (Figure 5E). And we also observed that compared to mouse DRG neurons, propionate could induce a mild Ca2+ influx in higher percentage of HEK 293 cells expressing hTRPV1, which only presented when propionate was applied prior to capsaicin stimulation but not after (Figures 5E and 3B). Thus, propionate exerted a reversible inhibitory effect on hTRPV1.

2.6 | Propionate inhibits hTRPV1 currents and interacts with the binding site in TRPV1

To further verify the potency of propionate, we performed electrophysiological recordings on HEK293 cells expressing hTRPV1. In accordance with what we learned from calcium imaging, concomitant perfusion of 100 μM propionate largely reduced capsaicin-activated currents. The dose–response curve yielded an IC_{50} of 20.08 ± 1.11 μM for inhibition of propionate on hTRPV1 activity (Figure 5F–I). We noticed that propionate alone did not evoke any ionic current (Figure 5G).

Next, we explored the putative interaction of propionate with the vanilloid binding site through molecular docking. The template structure and residues were analyzed to construct the homology modeling of hTRPV1 for docking, and the binding site of native ligand was selected around residue F543, M547, N551, Y511, S512,

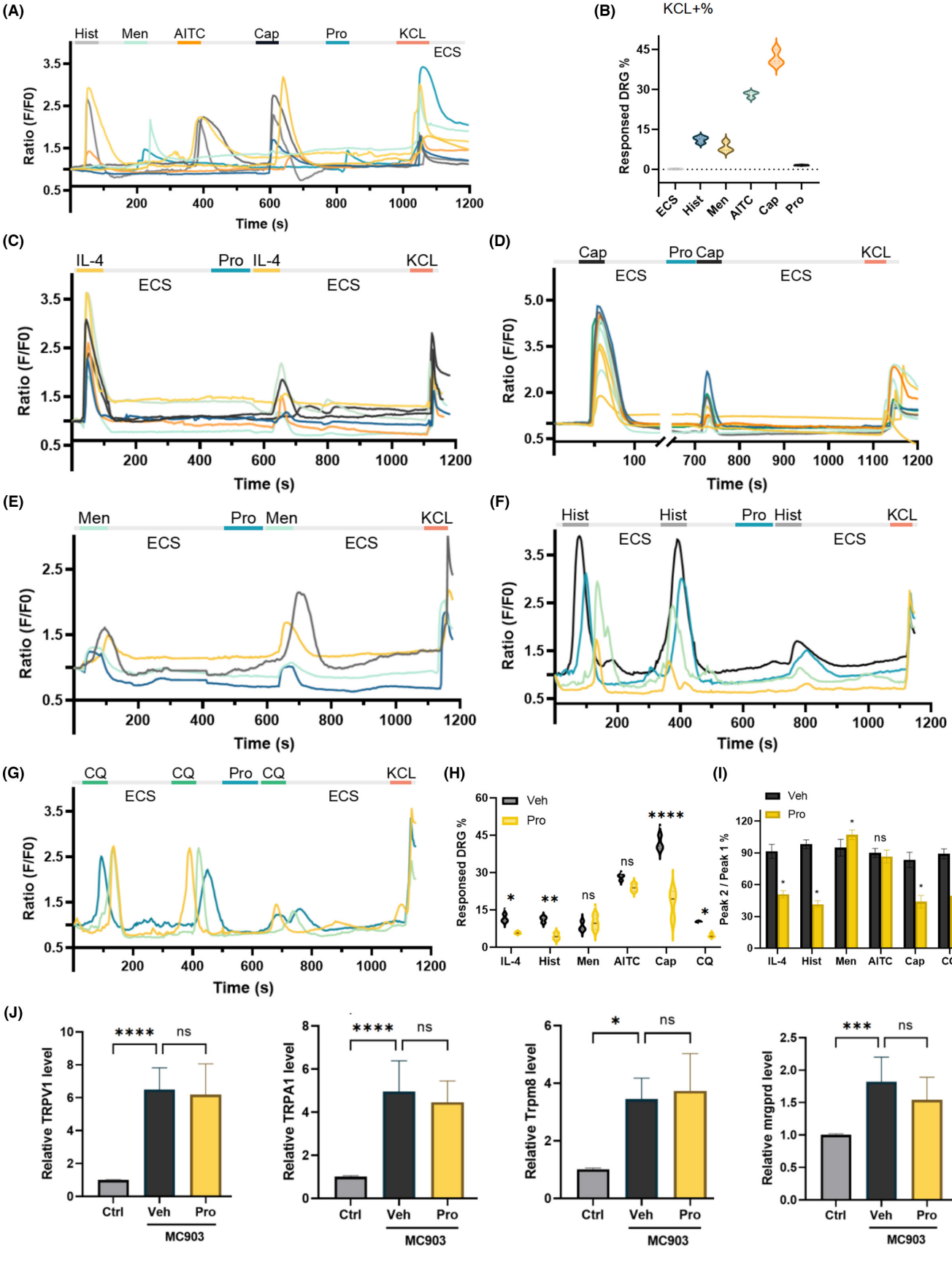

FIGURE 3 Propionate regulates mouse DRG neuron directly. (A) Calcium (Ca^{2+}) traces of representative DRG neurons (colored separately for identification) stimulated with histamine, menthol, AITC, capsaicin, propionate, or KCL. (B) Percent of total excitable (KCL responsive) DRG neurons responding to the indicated treatments. (C–G) Representative calcium imaging trace of mouse DRG neurons responding to IL-4, capsaicin, menthol, histamine, or chloroquine after treatment with propionate. (H) Changes in percentage of DRG neurons responding to the indicated treatments with or without propionate. (I) Propionate-affected magnitude of calcium influx in DRG neurons induced by the indicated treatments. (J) Relative expression of TRPV1, TRPA1, TRPM8, and Mrgprd in MC903 mice treated with or without propionate. $N > 500$ DRG neurons from 5 to 10 WT mice. Data are represented as mean ± SEM, one-way ANOVA followed by Tukey honest significant difference post hoc correction for multiple comparisons (B, J), paired *t*-test (H, I), ns = no significance, $^{*}p < .05$, $^{**}p < .01$, $^{***}p < .001$ and $^{****}p < .0001$. AITC, Allyl-isothiocyanate; Cap, capsaicin; CQ, chloroquine; Ctrl, control; ECS, extracellular solution; Hist, histamine; Men, menthol; Pro, propionate; Veh, vehicle control.

and R557 according to previous studies.[32] Within the binding pocket, the oxygen atom on the hydroxide of propionate, regarded as hydrogen bond donor, formed a hydrogen bond with the oxygen atom of Leu553 in TRPV1, and the oxygen atom on the carboxide of propionate, regarded as hydrogen bond acceptor, formed hydrogen bonds with the nitrogen atom of Gln701 in TRPV1. Van der Waals interactions were formed among propionate and the surround residues (Figure 5J). Similar docking strategy was applied for hTRPM8, which revealed that propionate formed a suitable steric complementarity with the binding site related to channel gating (Figure S6).[33]

For further validation, *Trpv1*$^{-/-}$ mice were utilized to produce the MC903-induced AD model in the lower hindlimb (Figure S7A). Compared with WT mice, *Trpv1*$^{-/-}$ mice demonstrated less scratching after MC903 application, which was equivalent to the MC903-treated mice receiving propionate (Figure S7B,C). Meanwhile, propionate alleviated skin inflammation in both WT and *Trpv1*$^{-/-}$ mice (Figure S7D,E). Taken together, these results suggested that propionate might act as a competitive capsaicin antagonist of TRPV1, and the protective effects of propionate in AD mice was at least partially due to the modulation of TRPV1.

2.7 | Propionate regulates CGRP release and attenuates skin inflammation

Neuropeptides are considered crucial effectors of sensory neurons interacting with immune system[24]; therefore, we sought to determine whether propionate could regulate the release of CGRP. As depicted in immunofluorescent images, the density of cutaneous nerve fibers co-labled with PGP 9.5 and CGRP was dramatically elevated in skin lesions of MC903 mice but profoundly decreased after propionate treatment ($p < .0001$), whereas no significant difference was observed between the AEW mice with or without propionate application ($p = .89$), indicating that CGRP was predominantly involved in inflammatory pruritus (Figure 6A,B). Other neuropeptides including substance P and neuromedin U were also detected, and the result showed that their mRNA expression levels remained unchanged in AEW model compared with control ($p = .07$, $p = .25$, Figure S8). CGRP protein expression in the skin tissues was then assayed by ELISA, and the result confirmed the findings of nerve fibers (Figure 6C). When dissociated DRG neurons were analyzed, the CGRP release elicited by capsaicin was markedly inhibited by either propionate or TRPV1-specific antagonist AMG-517, and the effect of combined administration was equivalent to that of each agent alone, which indicated that the regulation of CGRP by propionate was at least partially dependent on TRPV1 (Figure 6D).

Another important question was how CGRP influenced the antipruritic effects of propionate in AD. We injected 0.5 μg CGRP in 200 μL PBS intradermally 30 min after MC903 topical application to restore the CGRP level in skin lesions (Figure 6E). The result showed that CGRP administration induced more evident scratching responses and alloknesis in MC903-treated mice. The antipruritic activity of propionate was impaired by CGRP administration (Figure 6F,G). Moreover, the therapeutic effects of propionate in skin inflammation were also impeded by CGRP, as shown by the decreased dermatitis score and epidermis thickness (Figure 6H–J). Importantly, transcriptional levels of inflammatory cytokines were markedly reduced by propionate. However, co-treatment with CGRP further aggravated relative expressions of IL-4, IL-5, and IL-17 (Figure 6K). These results suggested that CGRP fueled itch and skin inflammation in AD.

3 | DISCUSSION

Pruritus is a defining and ubiquitous symptom of AD, which significantly affects the quality of life[34,35]; however, the control on itch is still suboptimal in most cases. The gut–microbiome–brain axis has been well established, and the neuro-immune crosstalk is implicated in various physiological and pathological processes; whereas the interactions between the skin microbiome and nervous system are far less recognized.[36] In the current study, we demonstrated that propionate, a microbial metabolite of sebum, alleviated both acute and chronic itch through sensory TRP channels in DRG neurons. Propionate also inhibited the secretion of CGRP by nerves in the MC903-induced AD mouse model, which further attenuated itch and skin inflammation. Our results revealed a microbiome-based mechanism for regulation of skin sensory nerves, and modulation of itch via the skin microbiome might be a novel strategy for the treatment of AD.

SCFAs are the most-studied microbial metabolites in the gut and have demonstrated important functions in both the immune and nervous system.[37] However, the importance of SCFAs in skin biology has just been recognized recently, and we reported a "sebum-propionate-IL-33" axis in the pathogenesis of AD.[19] The sebum can serve as a substrate for skin microbiota-mediated lipid metabolism, which results

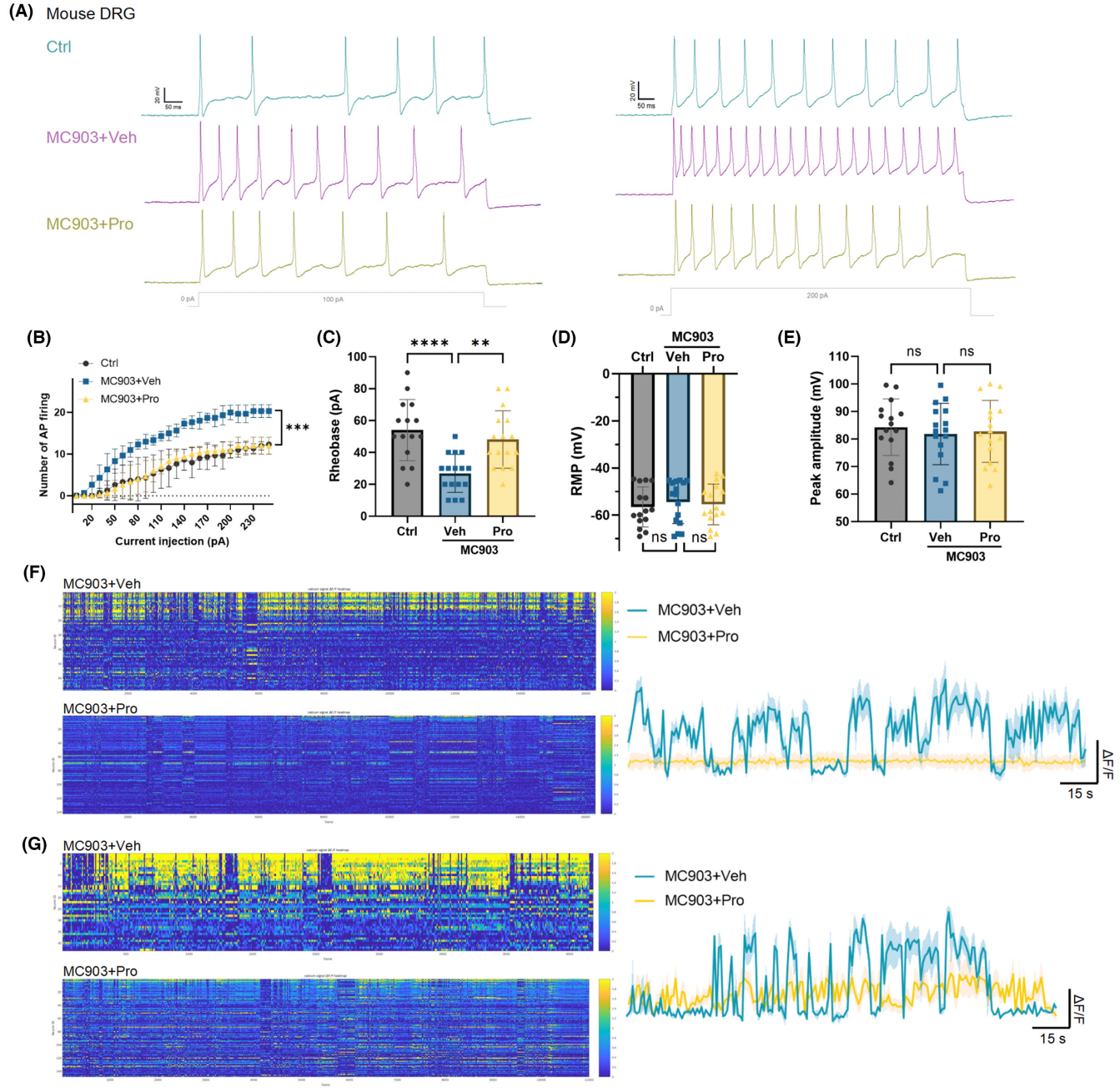

FIGURE 4 Propionate affects excitability of mouse DRG neurons. (A) Representative responses of DRG neurons from MC903 mice or control with or without propionate treatment to 1 s 0-250pA current pulse injection. Protocol of injected current is shown underneath. (B) Comparison of averaged frequency of action potential (AP) firing (numbers of action potential firing) evoked by current injection in DRG neurons. (C) Statistics plot showing resting membrane potential (RMP) from DRG neurons. (D) Summary of peak amplitude in DRG neurons responding to current pulse injection. (E) Action potential threshold in current-clamped DRG neurons among different groups. (F) Heatmap of representative neuronal Ca^{2+} activities in an awake, freely moving MC903 mouse treated with vehicle control (top, $n = 83$ cells) or propionate (bottom, $n = 142$ cells). And the averaged Ca^{2+} traces are shown on the right (blue line, MC903 + Veh; yellow line, MC903 + Pro). Data were derived from one animal and are representative of three similar experiments in $n = 4$ mice. (G) Heatmap of representative neuronal Ca^{2+} activities in MC903 mouse with a 3 cm piece of adhesive tape affixed to the hindlimb (within the skin lesion area), treated with vehicle control (top, $n = 68$ cells) or propionate (bottom, $n = 145$ cells). And the averaged Ca^{2+} traces are shown on the right (blue line, MC903 + Veh; yellow line, MC903 + Pro). Data were derived from one animal and are representative of three similar experiments in $n = 4$ mice. $N = 10$–15 cells/group (A–E), data are represented as mean ± SEM, two-way ANOVA followed by Bonferroni honest significant difference post hoc test (B), one-way ANOVA followed by Bonferroni post hoc test for multiple comparisons (C–E), ns = no significance, $^{*}p < .05$, $^{**}p < .01$, $^{***}p < .001$. Ctrl, control; Pro, propionate; Veh, vehicle control. See also Figure S5, Videos S1 and S2.

in the production of SCFAs. We have shown that the production of sebum and its microbial metabolite, propionate, are significantly decreased on the skin surface of AD patients compared to healthy individuals.[19] The effect of SCFAs on peripheral nerves has been reported and circulating SCFAs derived from the gut microbiota have been shown to attenuate nerve injury-associated neuropathic pain.[38] We speculated that propionate might be involved in elicitation or regulation of itch, and utilized several mouse models to test our hypothesis. The result showed that spontaneous scratching bouts induced by acute pruritogens were significantly reduced by intradermal application of propionate. The itch alleviation effect was further verified in a mouse model of chronic itch, in which improved skin inflammation and a decreased density of intraepidermal nerve fiber were also observed. To minimize the interference by skin inflammation, the AEW model was utilized, and propionate inhibited itch and decreased dermatitis score and epidermal thickness that are secondary to itch. Our findings update the understanding on the role of SCFAs in skin biology. Propionate can exert various effects on keratinocytes, immune cells, and DRG neurons and may participate in the pathogenesis of not only AD but also other skin diseases.[39,40]

Our study demonstrated for the first time that SCFA exerted its effects directly on DRG neurons. Previous study has reported that SCFAs regulate secretions of neurotransmitters and activate vagal afferents, thereby affecting food-intake, learning, memory, and emotion.[41] While our result showed that propionate reduced the responsiveness of DRG neurons in vitro to various pruritogens including IL-4. Because DRG are highly heterogeneous, only a small portion of DRG responded to propionate in our study. In in vivo experiment, intrathecal injection of propionate also exerted sufficient inhibitory effects without eliciting any nocifensive behaviors. We further revealed that propionate altered the responsiveness of DRG neurons to other pruritogens. The hyper-excitability of sensory neurons from MC903 mice were also restored by propionate treatment. As previous studies have shown that SCFAs participate in systemic inflammation as endogenous ligands for FFARs,[42] we first explored the role of FFAR in propionate-induced inhibition of itch. Using AAV-mediated FFAR3 genetic knockdown in DRG neurons, we found that the suppression of itch and alloknesis by propionate was not abolished in the absence of FFAR3. Despite the high expression of FFAR3 in sympathetic, vagal ganglia, or rat brain,[43] our data showed that the levels of FFAR3 mRNA transcript in the skin, DRG, and spinal cord were extremely low, in consistent with the results from the FFAR3 reporter mouse model (Ffar3+/mRFP).[31] These data indicate that the protective effect of propionate against pruritus through sensory neurons is largely independent of FFAR3. Additional work is needed to fully clarify the distribution and function of FFARs in nervous system.

Our data that propionate-responsive DRG also responded to menthol and capsaicin suggested that the effects of propionate might be associated with TRPV1 and TRPM8 channels. We then transfected HEK 293 cells with recombinant TRP channels and found that propionate activated TRPM8, desensitized TRPV1, and inhibited hTRPV1 currents induced by capsaicin with micromolar potency, as evidenced by calcium imaging and whole-cell patch clamp recordings. Moreover, propionate may interact with the capsaicin binding site in hTRPV1 through molecular docking. These findings encouraged us to regard propionate as a direct modulator of TRP channels. TRPV1 has been implicated in AD, psoriasis, allergic contact dermatitis (ACD), and wound healing.[44] In a psoriasis model induced by imiquimod, ablation of TRPV1+ cutaneous sensory nerves attenuates inflammation, reduces dendritic cells infiltration, and inhibits IL-23 production.[45] In the oxazolone-induced AD-like murine model, TRPV1 antagonist PAC-14028 alleviates the skin inflammation through blocking of IL-4 and IL-13 signaling.[46] A recent study demonstrates that TRPV1 promotes persistent itch in squaric acid dibutylester (SADBE)-induced ACD.[47] Besides, it has been reported that the cooling-inhibited pruritus is dependent on TRPM8 activation.[28] However, many of the antagonists for TRP channels have failed in clinical trials due to unexpected side-effects encompassing burning sensation and short-acting effect.[48] An important feature of our data is that propionate diminished both acute and chronic itch without inducing hyperthermia or other irritating responses, suggesting that propionate has a therapeutic potential for AD.

CGRP is intimately associated with atopic diseases, acting as the bridge between nervous and immune system.[49] Compared with non-lesional skin, $CGRP^+$ nociceptive nerves increasingly innervate the epidermis of AD lesion and are anatomically adjacent to immune cells, setting the foundation for augmentation of Th2 inflammatory responses.[50] Lack of CGRP signaling impedes type 2 immunity in allergic asthma.[51] CGRP can also shift antigen presentation toward Th2 responses, resulting in up-regulated production of IL-4 and IL-13 by T cells.[52,53] Interestingly, the plasma level of CGRP is significantly elevated in AD patients with severe pruritus in contrast to those with mild pruritus.[54] Conversely, a recent study reports that CGRP constrains Th2 inflammatory responses following helminth infection,[55] which indicates that CGRP might has complex and contradictory roles in the context of different microenvironment. In our model, we confirmed that CGRP amplified itch and exacerbated skin inflammation of AD model. We further found that propionate reduced the number of intradermal CGRP-positive nerves and inhibited CGRP release from DRG neurons partially through TRPV1 channel. However, because of the variabilities in route and amount of administration, CGRP might have different effects in different phases of AD.

Collectively, we characterized the regulatory role of skin microbial metabolite, propionate, in itch sensation through neuro-immune interaction for the first time. Our study highlighted the crosstalk between skin microbiome and sensory nerves as well as immune system, suggesting more convenient and effective approaches for AD itch management through a microbiome-based strategy.

4 | MATERIALS AND METHODS

4.1 | Mice

All animal experimental procedures were approved by the Animal Study Committee of Huashan Hospital, Fudan University and were conducted strictly following the guidelines for the ethical treatment

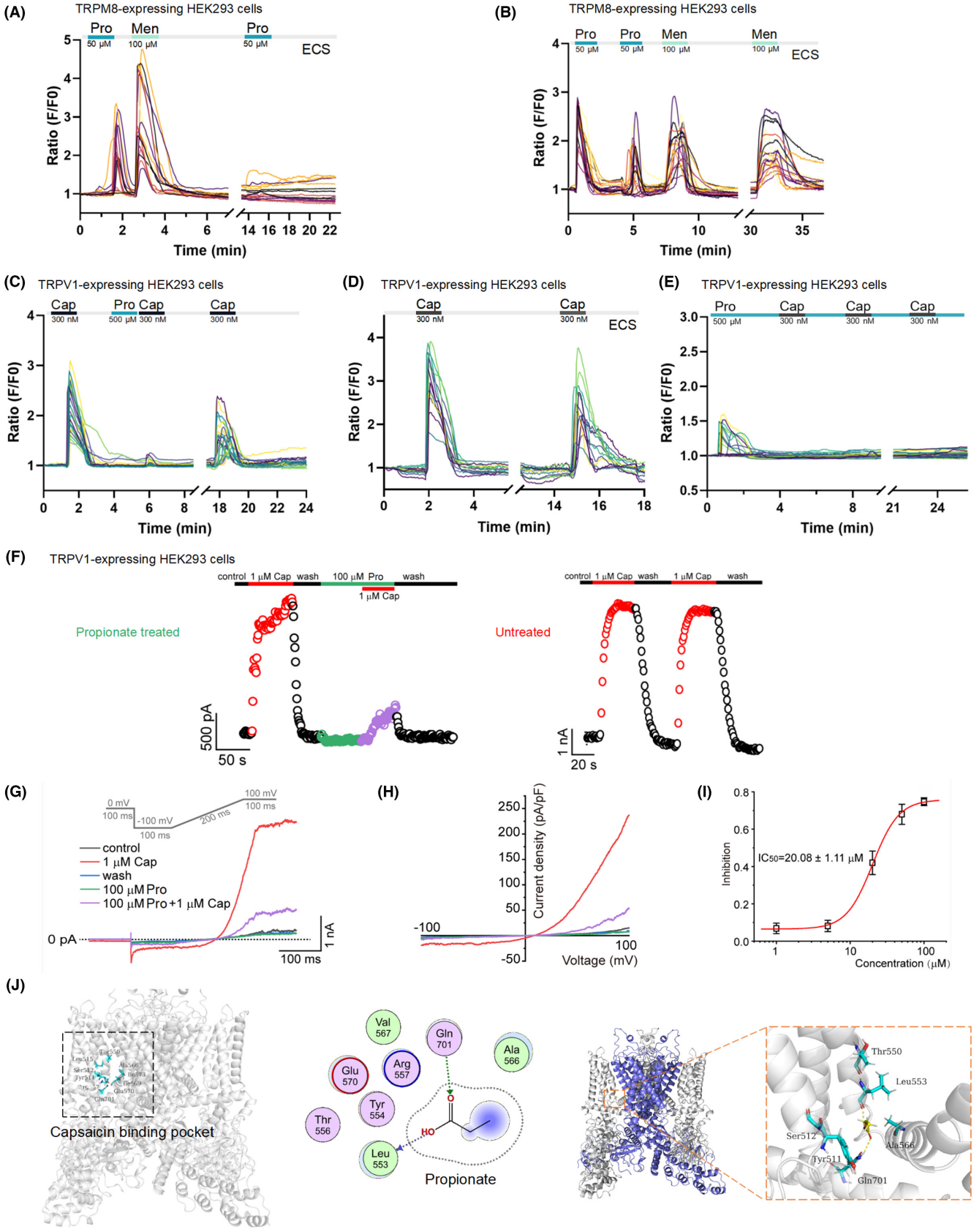

of animals. Batches of C57BL/6J mice (6–8 weeks, male and female) were purchased from Shanghai Laboratory Animal Center, Chinese Academy of Sciences (Shanghai, China) and maintained in a temperature and humidity-controlled (22°C–25°C, 45%–70%) specific pathogen free environment with a 12 h light/12 dark cycle. *Trpv1*$^{-/-}$ mice in the background of *C57BL/6J* were a generous gift

FIGURE 5 Propionate modulates hTRPV1 and hTRPM8 channels. (A, B) Representative time-lapse traces illustrate propionate and menthol-elicited $[Ca^{2+}]i$ responses in HEK293 cells transfected with hTRPM8 constructs. (C–E) Representative calcium influx in hTRPV1-transfected HEK293 cells stimulated with propionate and capsaicin. (F, G) Representative whole-cell currents evoked by 1 μM capsaicin in the absence and presence of 100 μM propionate in HEK293 cells expressing human TRPV1. (H) Current–voltage relations for data in (F, G). Current amplitudes were normalized to the maximum responses. (I) Dose–response curve for propionate on inhibition of hTRPV1. Red line represents a fit to a Hill equation, yielding $IC_{50} = 20.08 \pm 1.11$ μM. (J) Structural analysis of TRPV1 modeling results and binding site of capsaicin in TRPV1 are shown. The 2D and 3D binding mode of propionate and TRPV1 is presented. The hydrogen bonds are depicted as yellow dashed lines. The surrounding residues in the binding pocket are colored in cyan. $N > 500$ cells, data are represented as mean ± SEM, one-way ANOVA for multiple comparisons, ns = no significance, $^{*}p < .05$, $^{**}p < .01$, $^{***}p < .001$. Cap, capsaicin; ECS, extracellular solution; Men, menthol; Pro, propionate. See also Figures S6 and S7.

from Dr. Fengxian Li's laboratory (Zhujiang Hospital, Southern Medical University). All knockout mice were backcrossed at least 10 times with *C57BL/6J* mice before experiments. Age-matched WT littermates were used as control. Mice were randomly grouped and acclimated for at least 1 week before performing any experiments, the results of which were collected blindly.

4.2 | Acute itch model

Mice received intradermal microinjections of propionate, phosphate-buffered saline (PBS), or pruritogens in the cheek or in the paw.[56] For test of pruritogen-induced acute itch behaviors, cheeks were shaved, and mice were habituated to the recording chambers at least 2 days before the test. On the day of experiment, mice were injected with 10 μL of 4 mM propionate or control PBS solution and placed in the recording chambers for 30 min. Mice were then removed from the chambers and given an intradermal injection in the cheek of 10 μL of the following pruritogens: histamine (100 μg), chloroquine (100 μg), compound 48/80 (20 μg), 5-HT (2 μg), all diluted in saline containing 3.5% dimethyl sulfoxide. Immediately after the pruritogen injections, mice were placed in the recording chambers and video-recorded for 30 min. To test whether propionate contributes to acute pain behavior (nocifensive behavior), mice were intraplantar injected with 4 mM propionate or control PBS solution. Immediately after the paw injection, mice were placed in the recording chambers and video-recorded. Time spent on nocifensive behavior (flinching and licking) was 5 min.

4.3 | MC903 model

For induction of AD-like inflammation and chronic itch, mice were topically treated once daily with 2 nmol of MC903 for 9 consecutive days on ears, backs or hind legs as previously described.[8] Mice in control group were treated with 20 μL ethanol. For propionate treatment, mice were applied with 30 μL of 4 mM sodium propionate (dissolved in a 7:3 mix solvent of 1,2-propanediol and isopropyl alcohol) 30 min after MC903 application once a day (MC903 + Pro); in the vehicle control group, 30 μL of the solvent was used (MC903 + Veh).[19] For CGRP administration, 0.5 μg CGRP (Bachem) in 200 μL PBS was injected intradermally at spread 5 sites in the area of skin lesion 30 min after MC903 topical application once a day, and vehicle group received 200 μL PBS injection; then the propionate group was immediately treated with 4 mM propionate as described above.

4.4 | AEW model

The acetone-ether-water (AEW) model of non-inflammatory itch was produced as previously described.[28] Briefly, the nape of mice was shaved 2 days ahead of treatment. Then a cotton immersed in a 1:1 mixture of acetone (Sigma-Aldrich) and ether (Sigma-Aldrich) was applied to the skin for 15 s. Immediately after that, a second cotton immersed in distilled water was applied to the neck for 30 s. Control groups were treated with distilled water only. Treatments were applied twice daily for five consecutive days and scratching behavior was measured 8 h after the last application.

4.5 | GPR41 knockdown

The AAV9-GPR41 shRNA and control vectors were produced and purified as previously reported (Genomeditech).[57] For intrathecal injection, mice were anesthetized, shaved, and disinfected. After placed in the prone position, the lumbar spine was exposed and the rostral portion of the third lumbar vertebra were partially removed. Then the Hamilton syringe was punctured into the gap between the L5/L6 level and carefully inserted into the subarachnoidal space. Slowly released 10 μL vector into the cerebrospinal fluid for more than 2 min to minimize leakage. Mice would be housed two more weeks before further experiments.

4.6 | Cell lines and transfection

HEK 293 cells (ATCC, CRL-1573) were obtained from the American Type Culture Collection (ATCC) to record calcium responses after transfection with hTRPV1 or hTRPM8 plasmids as previously described.[58] Cells were grown in DMEM medium (4500 mg/L glucose) containing 10% fetal bovine serum, 2 mM L-glutamine, 100 IU/mL penicillin, and 100 μg/mL streptomycin, in a 100% humidity atmosphere with 5% CO2 at 37°C. Cells were transfected with 1 μg plasmid per 35-mm dish or 3 μg plasmid per 60-mm dish using Lipofectamine 3000 Transfection Reagent (Thermos Fisher).[59] The transfection

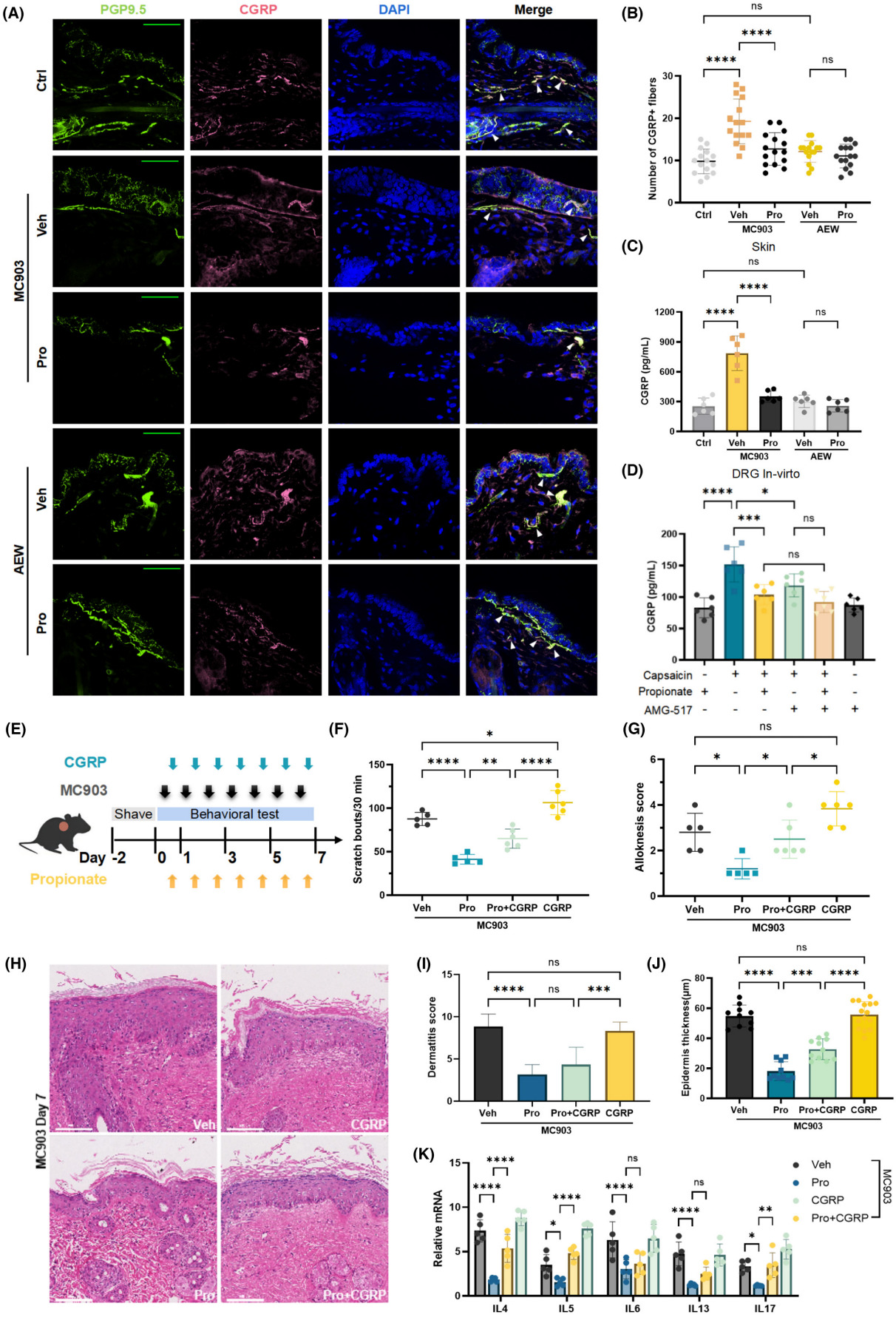

FIGURE 6 Propionate regulates CGRP release and prevents skin inflammation. (A, B) Immunofluorescence of nerve fibers. Representative immunofluorescent images of cutaneous peripheral nerve fibers stained with CGRP (violet), PGP9.5 (green), and DAPI (blue) are shown in (A) (Scale bar = 50 μm). Statistical result for calculation of intradermal CGRP-positive nerves is shown in (B). (C) CGRP protein release levels in ex vivo skin from MC903 and AEW mice treated with propionate or vehicle control. (D) CGRP protein release levels in cultured DRG neurons incubated with propionate, capsaicin, and (or) AMG-517. (E) Experimental schema of daily applications with MC903, propionate, and (or) CGRP. (F) Time courses of the numbers of spontaneous scratching bouts among different groups. (G) Representative alloknesis scores in mice from different groups. (H) H&E histopathology of skin tissues (Scale bar = 100 μm). (I, J) Calculation of histology score and epidermis thickness measurement. (K) Relative mRNA levels of inflammatory factors in mouse skin lesions. $N = 6$ mice/group, data are represented as mean ± SEM, one-way ANOVA followed by Tukey honest significant difference post hoc test for multiple comparisons, ns = no significance, $^{*}p < .05$, $^{**}p < .01$, $^{***}p < .001$ and $^{****}p < .0001$. AEW, acetone-ether-water; CGRP, Calcitonin gene-related peptide; Ctrl, control; Pro, propionate; Veh, vehicle control.

efficiency was confirmed by visualizing mCherry fluorescence after 24–48 h of incubation.

4.7 | Primary mouse DRG neuron culture

DRGs isolated from the C57BL/6J mice were cultured using a previously described protocol.[60] Briefly, laminectomies were performed on mice to dissect out bilateral DRGs and then digested with oxygenated DMEM containing collagenase (0.4 mg/mL), trypsin (1 mg/mL), and DNase (0.1 mg/mL) for 30 min in 37°C water bath. Neurons were gently triturated, resuspended in DMEM/F12 (1:1) media supplemented with 100 U/mL penicillin, 0.1 mg/mL streptomycin, and 10% fetal bovine serum. DRGs were then plated onto poly-D-lysine-coated glass coverslips and kept in a humidified incubator at 37°C for at least 24 h.

4.8 | Evaluation of scratching behavior

For spontaneous itch, mice were acclimated to the test environment daily for at least 3 days prior to testing, and itch was assessed by videotaping the mice for 30 min and then scored by a researcher blind to treatment. Spontaneous itch was determined by the number of scratching bouts, and a bout was defined as one rapid back-and-forth hind paw motion directed toward and contacting the treated region, ending with placement of the hind paw back to the floor or in the animal's mouth. Hind paw movements directed away from the injection site and grooming movements were not counted.[8] As for chronic itch model treated on the lower hindlimb, biting at the pruritic stimulation area was regarded as itch, whereas licking at the injection area reflected pain.[61]

For alloknesis, mice received five separate innocuous mechanical stimuli delivered using a von Frey filament (bending force: 0.07 g; Stoelting, Wood Dale, IL) to 5 randomly selected sites along the border of the cream application area. The presence or absence of a positive response (a hind limb scratching bout directed to the site of mechanical stimulation) was noted for each stimulus. The alloknesis score was the total number of positive responses elicited by the five stimuli (0–5).[62]

For tape response assay, mice were acclimated to the test environment for 1 h, then a 3 cm piece of common lab tape was gently applied to the skin lesion. Mice were video-recorded to count the total number of responses to the adhesive tape including biting and scratching until the tape was removed from the skin.[30]

4.9 | Behavior tests for somatomotor and nociception

Rotarod test: Mice were placed on a rotarod with the velocity increasing from 4 to 30 rpm within 5 min. The mouse was pretrained for 2 days before the formal test. The duration time before the mouse fell off the rotarod was recorded.[63]

Von Frey test: Mice were habituated in recording chambers for at least 1 h and the mechanical threshold was assessed by measuring the 50% paw withdrawal with a series of von Frey filaments applied to the left hindpaw. One filament was tested at most five times with 10 s interval in a round of experiment.[64]

Hargreaves test: Mice were acclimated in recording chambers for at least 1 h ahead of time, the radiant light was applied to the hind paw of mice when they were resting quietly, and the latency of paw withdraw was recorded. The cutoff time of radiant light stimulation was set at 20 s.[63]

4.10 | Histological analysis

Skin lesions from different groups were dissected and fixed overnight in 4% PFA. The sections were stained with hematoxylin/eosin (HE) according to the manufacture instructions.[45] The thickness of epidermis was measured in microns from the basement membrane to the top of the stratum corneum using ImageJ analysis software as previously described.[62]

To assess the nerve fiber density of epidermis, skins were snap-frozen in isopentane incubated in liquid nitrogen and sectioned into 10 μm slices. Tissue sections were fixed in acetone at room temperature for 20 min, permeabilized with 0.2% Triton X-100 in PBS, and then blocked with 3% bovine serum albumin, 0.2% Triton X-100, and 0.2% Tween 20 in PBS for 20 min. The sections were then stained with anti-PGP 9.5 (Abcam, Cat# ab108986, RRID:AB_10891773), anti-CGRP (Thermo Fisher, Cat# PA1-85250, RRID:AB_2259435), anti-NeuN (Abcam, Cat# ab177487, RRID:AB_2532109), and anti-TRPV1 (Thermo Fisher,

Cat# PA1-748, RRID:AB_2209010) primary antibodies at 4°C overnight and incubated with the secondary antibody (Abcam, Cat# ab150077, RRID:AB_2630356; Thermo Fisher, Cat# A-21447, RRID:AB_2535864) and DAPI (Thermo Fisher, Cat# 62248) for 30 min at room temperature. Images were obtained by a Nikon fluorescent microscope to evaluate the intraepidermal nerve fiber density (IENFD) via the ImageJ software. At least five random photographs were taken per specimen and the number of intradermal PGP9.5-positive nerves was counted and calculated per high-power field.[9]

4.11 | Evaluation of skin lesions

The clinical severity of dermatitis was evaluated at every timepoint of reagent application. The development of (1) erythema/hemorrhage, (2) scaling/dryness, (3) edema, and (4) excoriation/erosion was scored as 0 (none), 1 (mild), 2 (moderate), or 3 (severe). The sum of the individual scores was defined as the dermatitis score of each mouse.[65]

4.12 | Quantitative RT-PCR

Total RNA was extracted from mouse tissue using the RNeasy RNA isolation Kit (Qiagen) according to manufacturer's instructions. The RNA (1 μg) was reverse-transcribed and the cDNA was synthesized in vitro using PrimeScript RT Reagent Kit (Takara). Reactions were conducted in a volume of 10 μL per reaction containing SYBR Green premix (Takara) and specific primers (Table S1) using StepOnePlus real-time PCR system following the manufacturer's instructions. Relative mRNA expression levels of different target gene compared to actin were calculated using ΔΔCt methods. Primer sequences used for each gene were selected from pre-validated PrimeTime qPCR Assays.

4.13 | ELISA assay

CGRP concentration was measured using CGRP EIA kit (Cayman Chemical). All procedures were performed according to the manufacturer's protocols. For detection of CGRP level from skin lesion in each group, a 12 mm skin punch biopsy was obtained from the treated skin of mice. The samples were incubated in the 24-well plates containing 1 mL DMEM at 37°C with gentle shaking (150 rpm) for 30 min.[62] Then the supernatant from the skin explants cultures was collected for the following ELISA assay.[62] For the measurement of CGRP secretion from primary sensory neurons, DRGs were incubated with 100 μM propionate, 1 nM AMG-517 or vehicle and then treated with 1 μM capsaicin for 2 h after adherence. Harvested the supernatant and centrifugated at 4°C, 1500 rpm for 20 min, then measured CGRP levels as protocol described.[62]

4.14 | Live-cell Calcium imaging

4 μM Fluo4 AM (Invitrogen) was used to loading cultured DRG neurons and TRP channel-expressing HEK293 cells at 37°C for 20 min. Before use, Fluo4-loaded cells were washed for at least 3 times with HBSS (Gibco) at room temperature. Respectively, DRG neurons were stimulated with 100 μM propionate, 300 nM IL-4, 50 μM histamine, 1 mM chloroquine, 300 nM capsaicin, 100 μM AITC, or 100 μM menthol and washout with extracellular solution (ECS, 130 mM NaCl, 3 mM KCl, 2.5 mM CaCl2, 0.6 mM MgCl2, 10 mM HEPES, 10 mM glucose, 1.2 mM NaHCO3, pH 7.45). Fluorescence was recorded at 488 nm excitation wavelengths using an inverted Nikon Ti-E microscope with NIS-Elements imaging software (Nikon Instruments). Fluo4 ratios (F/F0) reflecting changes in $[Ca^{2+}]i$ upon stimulation were monitored and recorded (F = peak fluorescence signal; F0 = mean fluorescence signal at baseline). Cells were considered responsive if they demonstrated a change in fluorescence ratio over 10% of baseline. Regions of interest cells were identified and analyzed with Visiview software. Only cells responsive to 50 mM KCL were calculated.[29]

4.15 | Electrophysiology

Whole-cell patch clamp recordings were performed at room temperature using an Axon 700B amplifier (Molecular Devices). For transfected cells, mCherry-expressing cells were selected by a microscope equipped with a filter set for mCherry visualization (Nikon Instruments Inc.). For DRG neurons, small diameter neurons obtained from L3-L5 bilateral DRGs were preferred in recording. Pipettes prepared for whole-cell patch clamp recordings were pulled from borosilicate glass with a with 2–5 MΩ resistance. The internal solution contained 30 mM NaCl, 120 mM KCL, 1 mM $MgCl_2$, 0.5 mM $CaCl_2$, 5 mM EGTA, 2 mM Mg^{2+}-ATP, and 10 mM HEPES with pH 7.4. Osmolarity was adjusted to 300 mOsm/L. To prevent Ca^{2+}–dependent desensitization of TRPV1 currents, a Ca^{2+}–free extracellular solution was applied (140 mM NaCl, 5 mM KCl, 0.5 mM EGTA, 1 mM $MgCl_2$, 10 mM glucose, 10 mM HEPES, pH 7.4). Holding at 0 mV, voltage ramp from −100 to +100 mV for 500 ms was used to record whole-cell current. Resting membrane potential was recorded with a gap free protocol for each neuron under the current clamp mode after stabilization (within 3 min). A neuron was counted only if the resting potential was more negative than −40 mV. Data were acquired via a Digidata 1440 A/D converter (Molecular Devices) at 50 kHz and filtered at 10 kHz. For current clamp recordings, the internal solution contained (in mM): 140 CsCl, 2.0 $MgCl_2$, 5 EGTA, and 10 HEPES, pH 7.4 (adjusted with CsOH). The external solution contained (in mM): 140 NaCl, 5 KCl, 3 EGTA, and 10 HEPES, pH 7.4 (adjusted with NaOH). Data were analyzed and plotted using Clampfit 10.3. The concentration-response curve was fitted with the logistic equation: $Y = Y_{min} + (Y_{max} - Y_{min})/(1 + 10\text{^}[(\log IC_{50} - X) \times \text{Hill slope}])$, where Y is the response at a given concentration, Y_{max} and Y_{min} are the

maximum and minimum responses, X is the logarithmic value of the concentration and Hill slope is the slope factor of the curve. IC_{50} is the concentration that inhibits a response halfway between Y_{max} and Y_{min}.[60]

4.16 | Miniature two-photon imaging

For miniature two-photon experiments, 300 nL mixture virus of AAV2/9-Syn-GCaMP6s (titer: 3.2×10^{12}) was injected into the spinal cord dorsal horn L4-L5. After 2 weeks of viral expression, a miniature hand-held cranial drill (RWD Life Science) was used to create a 4 mm diameter window centered on the spinal cord directly above the virus injection site. A 4 mm glass slide (thickness: 100 μm) was then inserted into the spinal cord window and glued to the spinal cord with biological tissue glue (3 M), a holder was then glued to the chronic spinal cord window formed by glass coverslip. At least a week after recovery, an imaging Baseplate was positioned over the spinal cord window and cemented with dental acrylic. The miniature two-photon microscope (FHIRM-TPM V2.0, Field of view: $420\times420\,\mu m^2$, Resolution: 1300 nm, working distance: 1000 μm) was detachable while its holder was mounted permanently onto a baseplate over the spinal cord window. The cover of protective glue (Kwik-Cast, WPI Inc) on the spinal cord window were removed before imaging. Baseplate and miniature two-photon microscope are then fitted together and locked with M2 screws. Imaging data was acquired using the imaging software (GINKGO-MTPM, Transcend Vivoscope Biotech) at a frame rate of 10 Hz (512 × 512 pixels) with a femtosecond fiber laser (35 mW at the objective, TVS-FL-01, Transcend Vivoscope Biotech). GCaMP6s was excited at 920 nm. Then we produced the MC903 model on the mouse lower hindlimb, mice were randomly divided into propionate (4 mM) treatment group (MC903 + Pro) and vehicle control (MC903 + Veh). Mice with the mounted baseplate-holder assembly were acclimated to a homecage (30 cm × 20 cm × 20 cm) for 1 week, followed by a 2 days training to adapt the fiber and cable. To perform the behavioral test, mice carrying the miniature two-photon microscope were allowed free movement and video-recorded for 30 min. Data extracted from videos were then analyzed with custom MATLAB software. For measurement of Ca^{2+} activity, ROI was automatically recognized by the algorithm and manually supplemented using ImageJ, Relative fluorescence changes (ΔF/F) was calculated by an annular ring subtraction method to determine the calcium transient.[57]

4.17 | Molecular docking

Models were computed by the SWISS-MODEL server homology modelling pipeline,[66] which relies on ProMod3, a comparative modelling engine based on OpenStructure. ProMod3 extracts initial structural information from the template structure. Insertions and deletions, as defined by the sequence alignment, were resolved by first searching for viable candidates in a structural database. Final candidates were then selected using statistical potentials of mean force scoring methods. If no candidates were found, a conformational space search was performed using Monte Carlo techniques. Non-conserved side chains were modelled using a backbone-dependent rotamer library. The optimal configuration of rotamers was estimated using the graph-based TreePack algorithm by minimizing the SCWRL4 energy function. As a final step, small structural distortions, unfavorable interactions, or clashes introduced during the modelling process were resolved by energy minimization. ProMod3 used the OpenMM library to perform the computations and the CHARMM27 force field for parameterization.

MOE3 Dock was used for molecular docking of compound with human TRPV1 and human TRPM8. The 2D structures of molecules were downloaded from PubChem and converted to 3D structures in MOE through energy minimization, as ligands. Prior to docking, the force field of AMBER10: EHT and the implicit solvation model of Reaction Field (R-field) were selected. The "induced fit" protocol was selected, in which the side chains of the binding site in receptor were allowed to move according to ligand conformations, and a constraint was applied on their positions. The weight used for tethering side chain atoms to their original positions was 10. First, all docked poses were ranked by London dG scoring function, then force field refinement was applied on the top 30 poses followed by a rescoring of GBVI/WSA dG scoring function. The conformation with the lowest binding free energy was finally identified as the best probable binding mode. The binding mode was visualized by PyMOL (www.pymol.org). The binding site of native ligand in human TRPV1 structure was selected around residue F543, M547, N551, Y511, S512, and R5574. The binding site of native ligand in human TRPM8 structure was selected around residue Y745, D802, G805, I838, R842, L843, and I8465.

4.18 | Statistical analysis

All data were analyzed with GraphPad Prism (version 9.2.0) and presented as mean ± SEM, and individual data points were shown in graphs as mentioned. Two-tailed unpaired Student's *t*-test was used to analyze statistical significance between two independent experimental groups. One-way ANOVA followed by Fisher's least significant difference post hoc correction was performed for comparison between three or more groups. Two-way ANOVA followed by Tukey honest significant difference post hoc test was used for comparison in multiple groups with two independent variables. Sample size and detailed statistical analysis of each experiment were described in figure legends. $p < .05$ was considered statistically significant.

AUTHOR CONTRIBUTIONS

Conceptualization: Wei Li and Xu Yao. Methodology: Yao Xu, Changlin Li, and Zhuoqiong Qiu. Investigation: Yao Xu, Zhuoqiong Qiu, Su Yu, and Shangshang Wang. Visualization: Yao Xu and Chaoying Gu. Funding acquisition: Xu Yao, Wei Li, Chaoying Gu,

and Shangshang Wang. Project administration: Wei Li and Xu Yao. Supervision: Wei Li and Xu Yao. Writing—original draft: Yao Xu and Wei Li. Writing—review and editing: all authors.

ACKNOWLEDGMENTS

We would like to thank Dr. Fengxian Li for providing the *Trpv1*$^{-/-}$ mice. We are also indebted to Prof. Zhen Li for invaluable suggestions to electrophysiology analysis. Thanks to The Nanjing Brain Observatory for its assistance in miniature two-photon microscope. The Graphical Abstract (GA) was drawn by Figdraw (www.figdraw.com).

FUNDING INFORMATION

This study was funded by the National Natural Science Foundation of China (82073446, 81972939, 82273531, 82003349, 82003357, and 82330098), Key Project of the Innovation Program of Shanghai Municipal Education Commission (2021-01-07-00-07-E00078), the Milstein Medical Asian American Partnership Foundation (W. Li), Nanjing Incubation Program for National Clinical Research Centre (2019060001), Key Project of Social Development in Jiangsu Province (BE2020632), Shanghai Municipal Commission of Health and Family Planning (No. 2023ZZ02018), and Shanghai Municipal Key Clinical Specialty (No. shslczdzk01002).

CONFLICT OF INTEREST STATEMENT

The authors declare no competing interests.

DATA AVAILABILITY STATEMENT

All data associated with this study are in the paper or the supporting information (Figure S1; Tables S1 and S2; Videos S1 and S2). Correspondence and requests for materials should be directed to, and will be fulfilled by, the Lead Contact, Wei Li (liweiderma@fudan.edu.cn).

ORCID

Xu Yao https://orcid.org/0000-0003-3509-4775

REFERENCES

1. Ralvenius WT, Neumann E, Pagani M, et al. Itch suppression in mice and dogs by modulation of spinal α2 and α3GABAA receptors. *Nat Commun*. 2018;9:3230. doi:10.1038/s41467-018-05709-0
2. Moniaga CS, Tominaga M, Takamori K. The pathology of type 2 inflammation-associated itch in atopic dermatitis. *Diagnostics*. 2021;11:2090. doi:10.3390/diagnostics11112090
3. Langan SM, Irvine AD, Weidinger S. Atopic dermatitis. *Lancet*. 2020;396:345-360. doi:10.1016/S0140-6736(20)31286-1
4. Czarnowicki T, He H, Krueger JG, Guttman-Yassky E. Atopic dermatitis endotypes and implications for targeted therapeutics. *J Allergy Clin Immunol*. 2019;143:1-11. doi:10.1016/j.jaci.2018.10.032
5. Yosipovitch G, Rosen JD, Hashimoto T. Itch: from mechanism to (novel) therapeutic approaches. *J Allergy Clin Immunol*. 2018;142:1375-1390. doi:10.1016/j.jaci.2018.09.005
6. Cohen JA, Wu J, Kaplan DH. Neuronal regulation of cutaneous immunity. *J Immunol*. 2020;204:264-270. doi:10.4049/jimmunol.1901109
7. Brunner PM, Guttman-Yassky E, Leung DYM. The immunology of atopic dermatitis and its reversibility with broad-spectrum and targeted therapies. *J Allergy Clin Immunol*. 2017;139:S65-S76. doi:10.1016/j.jaci.2017.01.011
8. Oetjen LK, Mack MR, Feng J, et al. Sensory neurons Co-opt classical immune signaling pathways to mediate chronic itch. *Cell*. 2017;171:217-228.e13. doi:10.1016/j.cell.2017.08.006
9. Feld M, Garcia R, Buddenkotte J, et al. The pruritus- and TH2-associated cytokine IL-31 promotes growth of sensory nerves. *J Allergy Clin Immunol*. 2016;138:500-508.e24. doi:10.1016/j.jaci.2016.02.020
10. Liu B, Tai Y, Achanta S, et al. IL-33/ST2 signaling excites sensory neurons and mediates itch response in a mouse model of poison ivy contact allergy. *Proc Natl Acad Sci*. 2016;113:E7572-E7579. doi:10.1073/pnas.1606608113
11. Paller AS, Kong HH, Seed P, et al. The microbiome in patients with atopic dermatitis. *J Allergy Clin Immunol*. 2019;143:26-35. doi:10.1016/j.jaci.2018.11.015
12. Yu J, Luo Y, Zhu Z, et al. A tryptophan metabolite of the skin microbiota attenuates inflammation in patients with atopic dermatitis through the aryl hydrocarbon receptor. *J Allergy Clin Immunol*. 2019;143:2108-2119.e12. doi:10.1016/j.jaci.2018.11.036
13. Uberoi A, Bartow-McKenney C, Zheng Q, et al. Commensal microbiota regulates skin barrier function and repair via signaling through the aryl hydrocarbon receptor. *Cell Host Microbe*. 2021;29:1235-1248.e8. doi:10.1016/j.chom.2021.05.011
14. Li W, Xu X, Wen H, et al. Inverse association between the skin and Oral microbiota in atopic dermatitis. *J Invest Dermatol*. 2019;139:1779-1787.e12. doi:10.1016/j.jid.2019.02.009
15. Chng KR, Tay ASL, Li C, et al. Whole metagenome profiling reveals skin microbiome-dependent susceptibility to atopic dermatitis flare. *Nat Microbiol*. 2016;1:16106. doi:10.1038/nmicrobiol.2016.106
16. Seiti Yamada Yoshikawa F, Feitosa de Lima J, Notomi Sato M, Álefe Leuzzi Ramos Y, Aoki V, Leao OR. Exploring the role of *Staphylococcus aureus* toxins in atopic dermatitis. *Toxins*. 2019;11:321. doi:10.3390/toxins11060321
17. Franke K, Wang Z, Zuberbier T, Babina M. Cytokines stimulated by IL-33 in human skin mast cells: involvement of NF-κB and p38 at distinct levels and potent Co-operation with FcεRI and MRGPRX2. *Int J Mol Sci*. 2021;22:3580. doi:10.3390/ijms22073580
18. Nakatsuji T, Chen TH, Narala S, et al. Antimicrobials from human skin commensal bacteria protect against *Staphylococcus aureus* and are deficient in atopic dermatitis. *Sci Transl Med*. 2017;9:eaah4680. doi:10.1126/scitranslmed.aah4680
19. Qiu Z, Zhu Z, Liu X, et al. A dysregulated sebum–microbial metabolite–IL-33 axis initiates skin inflammation in atopic dermatitis. *J Exp Med*. 2022;219:e20212397. doi:10.1084/jem.20212397
20. Dalile B, Van Oudenhove L, Vervliet B, Verbeke K. The role of short-chain fatty acids in microbiota–gut–brain communication. *Nat Rev Gastroenterol Hepatol*. 2019;16:461-478. doi:10.1038/s41575-019-0157-3
21. Silva YP, Bernardi A, Frozza RL. The role of short-chain fatty acids from gut microbiota in gut-brain communication. *Front Endocrinol*. 2020;11:25. doi:10.3389/fendo.2020.00025
22. Goswami C, Iwasaki Y, Yada T. Short-chain fatty acids suppress food intake by activating vagal afferent neurons. *J Nutr Biochem*. 2018;57:130-135. doi:10.1016/j.jnutbio.2018.03.009
23. Shirolkar P, Mishra SK. Role of TRP ion channels in pruritus. *Neurosci Lett*. 2022;768:136379. doi:10.1016/j.neulet.2021.136379
24. Mikami N, Matsushita H, Kato T, et al. Calcitonin gene-related peptide is an important regulator of cutaneous immunity: effect on dendritic cell and T cell functions. *J Immunol*. 2011;186:6886-6893. doi:10.4049/jimmunol.1100028
25. Granstein RD, Wagner JA, Stohl LL, Ding W. Calcitonin gene-related peptide: key regulator of cutaneous immunity. *Acta Physiol*. 2015;213:586-594. doi:10.1111/apha.12442

26. Järvikallio A, Harvima IT, Naukkarinen A. Mast cells, nerves and neuropeptides in atopic dermatitis and nummular eczema. *Arch Dermatol Res*. 2003;295:2-7. doi:10.1007/s00403-002-0378-z
27. Oetjen LK, Kim BS. Interactions of the immune and sensory nervous systems in atopy. *FEBS J*. 2018;285:3138-3151. doi:10.1111/febs.14465
28. Palkar R, Ongun S, Catich E, et al. Cooling relief of acute and chronic itch requires TRPM8 channels and neurons. *J Invest Dermatol*. 2018;138:1391-1399. doi:10.1016/j.jid.2017.12.025
29. Perner C, Flayer CH, Zhu X, et al. Substance P release by sensory neurons triggers dendritic cell migration and initiates the Type-2 immune response to allergens. *Immunity*. 2020;53:1063-1077.e7. doi:10.1016/j.immuni.2020.10.001
30. Ranade SS, Woo SH, Dubin AE, et al. Piezo2 is the major transducer of mechanical forces for touch sensation in mice. *Nature*. 2014;516:121-125. doi:10.1038/nature13980
31. Colina C, Puhl HL, Ikeda SR. Selective tracking of FFAR3-expressing neurons supports receptor coupling to N-type calcium channels in mouse sympathetic neurons. *Sci Rep*. 2018;8:17379. doi:10.1038/s41598-018-35690-z
32. Caballero J. Computational modeling to explain why 5,5-Diarylpentadienamides are TRPV1 antagonists. *Molecules*. 2021;26:1765. doi:10.3390/molecules26061765
33. Xu L, Han Y, Chen X, et al. Molecular mechanisms underlying menthol binding and activation of TRPM8 ion channel. *Nat Commun*. 2020;11:3790. doi:10.1038/s41467-020-17582-x
34. Li H, Zhang Z, Zhang H, Guo Y, Yao Z. Update on the pathogenesis and therapy of atopic dermatitis. *Clin Rev Allergy Immunol*. 2021;61:324-338. doi:10.1007/s12016-021-08880-3
35. Cevikbas F, Lerner EA. Physiology and pathophysiology of itch. *Physiol Rev*. 2020;100:945-982. doi:10.1152/physrev.00017.2019
36. Yosipovitch G, Berger T, Fassett MS. Neuroimmune interactions in chronic itch of atopic dermatitis. *J Eur Acad Dermatol Venereol*. 2019;34:239-250. doi:10.1111/jdv.15973
37. Cryan JF, O'Riordan KJ, Cowan CSM, et al. The microbiota-gut-brain Axis. *Physiol Rev*. 2019;99:1877-2013. doi:10.1152/physrev.00018.2018
38. Bonomo RR, Cook TM, Gavini CK, et al. Fecal transplantation and butyrate improve neuropathic pain, modify immune cell profile, and gene expression in the PNS of obese mice. *Proc Natl Acad Sci*. 2020;117:26482-26493. doi:10.1073/pnas.2006065117
39. Trompette A, Pernot J, Perdijk O, et al. Gut-derived short-chain fatty acids modulate skin barrier integrity by promoting keratinocyte metabolism and differentiation. *Mucosal Immunol*. 2022;15:1-19. doi:10.1038/s41385-022-00524-9
40. Schwarz A, Philippsen R, Schwarz T. Induction of regulatory T cells and correction of cytokine disbalance by short-chain fatty acids: implications for psoriasis therapy. *J Invest Dermatol*. 2021;141:95-104.e2. doi:10.1016/j.jid.2020.04.031
41. Liu X, Li X, Xia B, et al. High-fiber diet mitigates maternal obesity-induced cognitive and social dysfunction in the offspring via gut-brain axis. *Cell Metab*. 2021;33:923-938.e6. doi:10.1016/j.cmet.2021.02.002
42. Kimura I, Ichimura A, Ohue-Kitano R, Igarashi M. Free fatty acid receptors in health and disease. *Physiol Rev*. 2020;100:171-210. doi:10.1152/physrev.00041.2018
43. Bartoszek A, Moo EV, Binienda A, et al. Free fatty acid receptors as new potential therapeutic target in inflammatory bowel diseases. *Pharmacol Res*. 2020;152:104604. doi:10.1016/j.phrs.2019.104604
44. Bagood MD, Isseroff RR. TRPV1: role in skin and skin diseases and potential target for improving wound healing. *Int J Mol Sci*. 2021;22:6135. doi:10.3390/ijms22116135
45. Riol-Blanco L, Ordovas-Montanes J, Perro M, et al. Nociceptive sensory neurons drive interleukin-23-mediated psoriasiform skin inflammation. *Nature*. 2014;510:157-161. doi:10.1038/nature13199
46. Lee JH, Choi CS, Bae IH, Choi JK, Park YH, Park M. A novel, topical, nonsteroidal, TRPV1 antagonist, PAC-14028 cream improves skin barrier function and exerts anti-inflammatory action through modulating epidermal differentiation markers and suppressing Th2 cytokines in atopic dermatitis. *J Dermatol Sci*. 2018;91:184-194. doi:10.1016/j.jdermsci.2018.04.017
47. Feng J, Yang P, Mack MR, et al. Sensory TRP channels contribute differentially to skin inflammation and persistent itch. *Nat Commun*. 2017;8:980. doi:10.1038/s41467-017-01056-8
48. Nikolaeva-Koleva M, Butron L, González-Rodríguez S, et al. A capsaicinoid-based soft drug, AG1529, for attenuating TRPV1-mediated histaminergic and inflammatory sensory neuron excitability. *Sci Rep*. 2021;11:246. doi:10.1038/s41598-020-80725-z
49. Pinho-Ribeiro FA, Baddal B, Haarsma R, et al. Blocking neuronal signaling to immune cells treats streptococcal invasive infection. *Cell*. 2018;173:1083-1097.e22. doi:10.1016/j.cell.2018.04.006
50. Russo AF, Hay DL. CGRP physiology, pharmacology, and therapeutic targets: migraine and beyond. *Physiol Rev*. 2022;103:1565-1644. doi:10.1152/physrev.00059.2021
51. Li J, Chen Y, Chen QY, et al. Role of transient receptor potential cation channel subfamily V member 1 (TRPV1) on ozone-exacerbated allergic asthma in mice. *Environ Pollut*. 2019;247:586-594. doi:10.1016/j.envpol.2019.01.091
52. Antúnez C, Torres MJ, López S, et al. Calcitonin gene-related peptide modulates interleukin-13 in circulating cutaneous lymphocyte-associated antigen-positive T cells in patients with atopic dermatitis. *Br J Dermatol*. 2009;161:547-553. doi:10.1111/j.1365-2133.2009.09318.x
53. Ding W, Stohl LL, Saab J, et al. Regulation of cutaneous immunity in vivo by calcitonin gene-related peptide signaling through endothelial cells. *J Immunol*. 2022;208:633-641. doi:10.4049/jimmunol.2100139
54. Salomon J, Baran E. The role of selected neuropeptides in pathogenesis of atopic dermatitis. *J Eur Acad Dermatol Venereol*. 2008;22:223-228. doi:10.1111/j.1468-3083.2007.02399.x
55. Nagashima H, Mahlakõiv T, Shih HY, et al. Neuropeptide CGRP limits group 2 innate lymphoid cell responses and constrains type 2 inflammation. *Immunity*. 2019;51:682-695.e6. doi:10.1016/j.immuni.2019.06.009
56. Jiang H, Cui H, Wang T, et al. CCL2/CCR2 signaling elicits itch- and pain-like behavior in a murine model of allergic contact dermatitis. *Brain Behav Immun*. 2019;80:464-473. doi:10.1016/j.bbi.2019.04.026
57. Zong W, Wu R, Chen S, et al. Miniature two-photon microscopy for enlarged field-of-view, multi-plane and long-term brain imaging. *Nat Methods*. 2021;18:46-49. doi:10.1038/s41592-020-01024-z
58. Than JYXL, Li L, Hasan R, Zhang X. Excitation and modulation of TRPA1, TRPV1, and TRPM8 channel-expressing sensory neurons by the pruritogen chloroquine. *J Biol Chem*. 2013;288:12818-12827. doi:10.1074/jbc.m113.450072
59. Kozisek T, Hamann A, Samuelson L, Fudolig M, Pannier AK. Comparison of promoter, DNA vector, and cationic carrier for efficient transfection of hMSCs from multiple donors and tissue sources. *Mol Ther Nucleic Acids*. 2021;26:81-93. doi:10.1016/j.omtn.2021.06.018
60. Yang L, Dong F, Yang Q, et al. FGF13 selectively regulates heat nociception by interacting with Nav1.7. *Neuron*. 2017;93:806-821.e9. doi:10.1016/j.neuron.2017.01.009
61. Akiyama T, Nagamine M, Carstens MI, Carstens E. Behavioral model of itch, alloknesis, pain and allodynia in the lower hindlimb and correlative responses of lumbar dorsal horn neurons in the mouse. *Neuroscience*. 2014;266:38-46. doi:10.1016/j.neuroscience.2014.02.005
62. Lee SH, Tonello R, Im ST, et al. Resolvin D3 controls mouse and human TRPV1-positive neurons and preclinical progression of psoriasis. *Theranostics*. 2020;10:12111-12126. doi:10.7150/thno.52135

63. Zhang S, Cai B, Li Z, et al. Fibroblastic SMOC2 suppresses mechanical nociception by inhibiting coupled activation of primary sensory neurons. *J Neurosci*. 2022;42:4069-4086. doi:10.1523/jneurosci.2132-21.2022
64. Wu D, Chen Y, Li Z, et al. *Zcchc12*-containing nociceptors are required for noxious heat sensation. *J Neurosci*. 2022;42:2690-2700. doi:10.1523/jneurosci.1427-21.2022
65. Al Kindi A, Williams H, Matsuda K, et al. *Staphylococcus aureus* second immunoglobulin-binding protein drives atopic dermatitis via IL-33. *J Allergy Clin Immunol*. 2021;147:1354-1368.e3. doi:10.1016/j.jaci.2020.09.023
66. Waterhouse A, Bertoni M, Bienert S, et al. SWISS-MODEL: homology modelling of protein structures and complexes. *Nucleic Acids Res*. 2018;46:W296-W303. doi:10.1093/nar/gky427

SUPPORTING INFORMATION

Additional supporting information can be found online in the Supporting Information section at the end of this article.

How to cite this article: Xu Y, Qiu Z, Gu C, et al. Propionate alleviates itch in murine models of atopic dermatitis by modulating sensory TRP channels of dorsal root ganglion. *Allergy*. 2024;00:1-20. doi:10.1111/all.15998